

# Adsorption Behavior of *n*-Hexanol on Ag(111) from Aqueous 0.05 M KClO<sub>4</sub>

Maria Luisa Foresti\* and Massimo Innocenti

Dipartimento di Chimica, Università di Firenze, Via G. Capponi 9, 50121 Firenze, Italy

Antoinette Hamelin

Laboratoire d'Electrochimie Interfaciale, CNRS, 1 Place A. Briand, 92195 Meudon Cedex, France

Received May 9, 1994. In Final Form: September 27, 1994\*

A computerized chronocoulometric technique was employed to investigate the adsorption behavior of *n*-hexanol (NHEX) on the (111) face of a silver single crystal from aqueous 0.05 M KClO<sub>4</sub>. The charge density,  $\sigma_M$ , as a function of the applied potential,  $E$ , and of the NHEX concentration was analyzed thermodynamically, yielding the Gibbs surface excess and the standard Gibbs energy of adsorption,  $\Delta G^{\circ}_{ads}$ , of NHEX as a function of  $E$  and  $\sigma_M$ . A comparison of the experimental adsorption parameters with a molecular model points to a flat orientation of the adsorbed NHEX molecules. The low value of  $-\Delta G^{\circ}_{ads}$  at the potential of maximum adsorption, 18.4 kJ mol<sup>-1</sup>, is indicative of the strongly hydrophilicity of silver.

## Introduction

Investigations of organic adsorption on solid metals are important from both a technological and a fundamental point of view. Thus, these researches may allow a better understanding of the mechanism of electrode processes in electrosynthesis and electrocatalysis, as well as a better control in the use of organics as corrosion inhibitors and polishing agents. Moreover, the adsorption of neutral organic compounds at electrodes provides valuable information on the structure of the interfacial region.

Quantitative investigations of the adsorption of uncharged organic molecules on single crystal electrodes are scanty and the majority of them were carried out on metals with low melting points such as Bi,<sup>1</sup> Sn,<sup>2</sup> Zn,<sup>3</sup> and Pb,<sup>4</sup> on the basis of differential capacity measurements and with an extrathermodynamic analysis of the experimental data. Differential capacity measurements often fail to yield realistic quantitative data<sup>5</sup> because of the lack of equilibrium at the interphase: this is the main reason why these measurements are hardly amenable to a thermodynamic analysis, which is quite demanding as to the accuracy and reproducibility to the data to be analyzed.

Results accurate enough to permit a satisfactory thermodynamic analysis have been more recently obtained by chronocoulometry, which allows reproducible adsorption measurements even if adsorption is very slow, provided that a small potential range is available where desorption is fast and complete. The differences in behavior on different single crystal faces are small for the low melting metals, probably due to a relatively high surface mobility.<sup>6</sup> Conversely, substantial differences are observed with Ag and Au. Chronocoulometry has been employed in the study of the adsorption of *tert*-pentyl alcohol, pyridine, diethyl ether, and benzonitrile on Au

single crystal faces and in that of pyridine on Ag single crystal faces.<sup>7</sup>

Quantitative investigations of the adsorption of simple aliphatic compounds are quite limited in number on Au single crystal faces.<sup>8</sup> No definite conclusions have yet been drawn<sup>7</sup> as to the effect of the different crystallographic orientations of Au on *tert*-pentyl alcohol adsorption.<sup>9,10</sup> More scarce results were published for Ag single crystal faces.

For adsorption of aliphatic compounds on Ag single crystal faces, no experimental data accurate enough to allow a thermodynamic analysis are presently available in the literature. Hinnen et al.<sup>11</sup> compared the differential capacity ( $C$ ) vs potential curves of 0.02 M NaF aqueous solutions saturated with ethyl ether on the three low-index faces of Ag with the same curves in the absence of ether. Ethyl ether does not affect the  $C$  vs  $E$  curve on Ag(110), thus indicating that its adsorption on this face is either vanishingly small or very slow even at the low frequency adopted (15 Hz). However, ethyl ether depresses the differential capacity on the Ag(111) and Ag(100) faces in the proximity of the potential of zero charge, this depression being slightly greater on Ag(111) than on Ag(100). The lack of a desorption peak on the positive side of the capacity minimum, which contrasts with the presence of a desorption peak on the negative side, was ascribed by the authors to slow desorption kinetics,<sup>11</sup> which is particularly pronounced at positive potentials. This prevented a quantitative estimate of diethyl ether adsorption on Ag from differential capacity measurements. Vitanov and Popov determined the adsorption isotherms of *n*-hexanol,<sup>12</sup> isobutyl alcohol,<sup>13</sup> and *n*-pentanol<sup>14</sup> on Ag(111) and Ag(100) at the potential of maximum adsorption from differential capacity measurements using an ex-

\* Abstract published in *Advance ACS Abstracts*, December 15, 1994.

(1) Paltusova, N. A.; Alumaa, A. R.; Palm, U. V. *Elektrokhimiya* 1979, 15, 1870.

(2) Kuprin, M. P.; Grigoryev, N. B. *Elektrokhimiya* 1980, 16, 383.

(3) Ipatov, Yu. P.; Batrakov, V. V. *Elektrokhimiya* 1975, 11, 1282.

(4) Khmelevaya, L. P.; Chizhov, A. V.; Damaskin, B. B.; Vainblat, T. I. *Elektrokhimiya* 1980, 16, 257.

(5) Nguyen Van Huong, C.; Hinnen, C.; Dalbera, J. P.; Parsons, R. *J. Electroanal. Chem.* 1981, 125, 177.

(6) Parsons, R. *J. Electroanal. Chem.* 1983, 150, 51.

(7) Lipkowski, J.; Stolberg, L. In *Adsorption of Molecules at Metal Electrodes*; Lipkowski, J., Ross, P. N., Eds.; Plenum Press: New York, 1992; p 171.

(8) Lipkowski, J.; Nguyen Van Huong, C.; Hinnen, C.; Parsons, R. *J. Electroanal. Chem.* 1983, 143, 375.

(9) Richer, J.; Stolberg, L.; Lipkowski, J. *Langmuir* 1986, 2, 630.

(10) Richer, J.; Lipkowski, J. *J. Electroanal. Chem.* 1988, 251, 217.

(11) Hinnen, C.; Nguyen Van Huong, C.; Dalbera, J. P. *J. Chim. Phys. (France)* 1982, 79, 37.

(12) Vitanov, T.; Popov, A. *Elektrokhimiya* 1974, 10, 1373.

(13) Vitanov, T.; Popov, A. *Elektrokhimiya* 1976, 12, 319.

(14) Popov, A.; Velev, O.; Vitanov, T. *J. Electroanal. Chem.* 1988, 256, 405.

trathermodynamic approach based on the two-parallel capacitor model. The adsorption of *n*-hexanol from 0.05 M Na<sub>2</sub>SO<sub>4</sub> was investigated on Ag single crystals grown electrolytically in a glass capillary; the single crystal faces exhibited a number of screw dislocations which were partially eliminated by electrodepositing Ag<sup>+</sup> ions at a 1 mV overpotential.<sup>12</sup> According to the authors, the time required to attain adsorption equilibrium at the potential of maximum adsorption was about 4 h for the most dilute alcohol solutions and 30 min for the saturated solution. After attaining these equilibrium conditions, the differential capacity was measured over the whole potential range without having to establish any further equilibrium conditions. In the adsorption measurements of isobutyl alcohol from 0.05 M Na<sub>2</sub>SO<sub>4</sub>, the Ag single crystal faces were electropolished anodically before use.<sup>13</sup> This procedure yielded reproducible positive desorption peaks and apparently reduced the time required for adsorption equilibrium to 30 min for the most dilute alcohol solutions and to 10 min for the most concentrated ones. Comparable times were required for *n*-pentanol adsorption from 0.1 M KF on Ag single crystals grown electrolytically in Teflon capillaries.<sup>14</sup> The absolute value of the Gibbs adsorption free energy of *n*-hexanol<sup>12</sup> was found to be slightly greater on Ag(111) than on Ag(100) ( $\Delta G^{\circ}_{111} = -24.6 \text{ kJ mol}^{-1}$  and  $\Delta G^{\circ}_{100} = -23.0 \text{ kJ mol}^{-1}$ ) whereas an opposite trend was reported for *n*-pentanol<sup>14</sup> ( $\Delta G^{\circ}_{111} = -15.0 \text{ kJ mol}^{-1}$  and  $\Delta G^{\circ}_{100} = -15.8 \text{ kJ mol}^{-1}$ ). The authors explained the slow attainment of adsorption equilibrium when shifting the potential from negative values to the potential of maximum adsorption by a slow adsorption on the growth steps of the silver surface. However, such a slow adsorption is apparently inconsistent with the sharp and high adsorption-desorption peaks reported by the authors on both sides of the flat differential capacity minimum.

### Experimental Section

The water used was obtained from bottled light mineral water by distilling it once and then distilling the water so obtained from acidic permanganate, while the heads were constantly discarded. Merck KClO<sub>4</sub> was recrystallized twice from bidistilled water and then dried. Fluka analytical reagent grade *n*-hexanol was distilled in an atmosphere of nitrogen before use. The alcohol concentrations was varied only from  $3.46 \times 10^{-3}$  to  $3.46 \times 10^{-2}$  M because for lower concentrations the capacitance-potential curves of the base electrolyte are not altered by addition of *n*-hexanol (NHEX), and no higher concentrations were studied because of solubility limits in 0.05 M KClO<sub>4</sub>. The solutions were freshly prepared just before the beginning of each series of measurements.

The working electrodes used in this work were cylindrical silver single crystals grown according to the Bridgeman technique in a graphite crucible, oriented by X-rays and cut<sup>15</sup> either in the Laboratoire d'Electrochimie Interfaciale du CNRS in Meudon-Bellevue (France) or in Florence, Italy. These electrodes were polished with successively finer grades of alumina powder down to 0.05 μm and then annealed in a muffle furnace at normal atmospheric pressure for 30 min at 650 °C. All electrochemical measurements were carried out in Florence. Before each experiment the electrode was polished chemically with CrO<sub>3</sub> according to the procedure described in ref 16. After polishing, the electrode surface was soaked in concentrated sulfuric acid for about 20 min and then rinsed thoroughly with water. The hanging solution method<sup>17</sup> was employed. The cylindrical single crystal electrode was held by a platinum wire sealed into a glass tube, which was secured to a movable stand; the latter was moved

up or down at an adjustable rate by means of an oleopneumatic piston which ensured the complete absence of vibrations. A pressure gauge connected to the oleopneumatic system permitted us to reproduce the optimum rate (1.5 mm/s). The stand was connected to a digital position sensor, which permitted us to estimate a 0.1 mm vertical shift of the stand. By this system the vertical position of the electrode, and hence the meniscus of the hanging solution, could be reproduced with a high accuracy.

The cell was water-jacketed and thermostated at  $25 \pm 0.2$  °C. A gold coil was used as a counter electrode and an external saturated calomel electrode (SCE) served as the reference. The four-electrode potentiostatic system by Herrmann et al.<sup>18</sup> was employed to minimize the noise. The wholly computerized instrumentation for differential capacity and charge measurements is described in the next section; positive feedback circuitry was utilized to compensate for the electrolyte resistance.

Before carrying out adsorption measurements, the state of the electrode surface in contact with an aqueous solution of 0.05 M KClO<sub>4</sub>, previously purged with argon for about 30 min, was checked by recording the curve of the differential capacity vs the applied potential at 20 Hz of ac modulation. Measurements were carried out only upon ascertaining the quantitative agreement of these curves with those reported in the literature.<sup>19</sup> Each set of differential capacity-potential curves and charge measurements at different alcohol concentrations was carried out while the single crystal face was maintained in constant contact with the solution through the meniscus. To this end the alcohol concentration in the cell was increased progressively by adding deaerated alcohol from a Hamilton microliter syringe into the previously deaerated aqueous solution of 0.05 M KClO<sub>4</sub>. The plunger of the syringe was fastened tightly to the rod of a digital-display micrometer screw of 0.005 mm pitch. The micrometer screw was held by a movable stand which permitted the syringe needle to be lowered into the solution during the addition and raised above the solution just after the addition. Before entering the cell, the argon used for the deaeration was bubbled in a vessel containing a solution of the same composition as that in the cell; this prevented both a change in the alcohol concentration in the cell and a decrease in the level of the solution surface which would have altered the shape of the meniscus. After each addition of the alcohol, the solution was stirred mildly with a magnetic stirrer for a time long enough to allow its complete dissolution (~20 min for the concentration at saturation,  $\sim 4 \times 10^{-2}$  M). For an accurate estimate of the stirring time necessary for the dissolution of the alcohol, charge vs potential curves were previously recorded on a pressurized static mercury drop electrode<sup>20</sup> at increasing stirring times until a constancy in these curves was attained. Argon was bubbled into the solution under study for a few minutes after each addition of the alcohol, whereas it was flowed over the solution during its complete dissolution in the solution and the subsequent measurements. After each addition, the differential capacity and the capacitive charge were recorded in succession as a function of the applied potential.

### Results

**Differential Capacity.** The curves of the differential capacity (*C*) against the applied potential (*E*) were recorded assuming a simple series RC equivalent circuit and are shown in Figure 1; an ac signal of 20 Hz and 5 mV rms was superimposed on the dc voltage ramp. In agreement with the literature<sup>19</sup> the curve of the supporting electrolyte shows a minimum due to the contribution of the diffuse layer at -0.746 V. At the low chosen KClO<sub>4</sub> concentration specific adsorption of this 1,1-valent electrolyte in the proximity of the minimum is negligible, and hence the potential of the minimum corresponds to the potential of zero charge (pzc).

The lowest concentrations of NHEX cause a modest depression of the differential capacity in the neighborhood of the minimum; this depression is clearly not compensated

(15) Hamelin, A. In *Modern Aspects of Electrochemistry*; Conway, B. E., White, R. E., Bockris, J. O'M., Eds.; Plenum Press: New York, 1985; Vol. 16, p 1.

(16) Hamelin, A.; Stoicovicu, L.; Doubova, L.; Trasatti, S. *J. Electroanal. Chem.* **1988**, *244*, 133.

(17) Dickertmann, D.; Schultze, J. W.; Koppitz, F. D. *Electrochim. Acta*, **1976**, *21*, 967.

(18) Herrmann, C. C.; Perrault, G. G.; Konrad, D.; Pilla, A. A. *Bull. Soc. Chim. Fr.* **1972**, *12*, 4468.

(19) Valette, G. *J. Electroanal. Chem.* **1989**, *269*, 191.

(20) Foresti, M. L.; Guidelli, R. *J. Electroanal. Chem.* **1986**, *197*, 159.

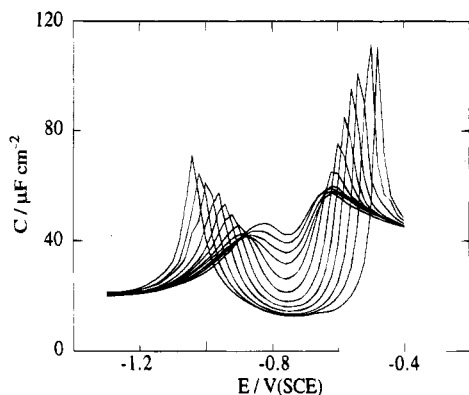


**Figure 1.** The first curve, as counted from top to bottom over the intermediate potential region, is the  $C$  vs  $E$  plot for the interface between Ag(111) and aqueous 0.05 M  $\text{KClO}_4$  in the absence of NHEX; the successive curves are relative to progressive additions of NHEX from  $3.46 \times 10^{-3}$  to  $3.46 \times 10^{-2}$  M by  $\log(c/M)$  increments of 0.1.

for by an equivalent increase with respect to the differential capacity of the supporting electrolyte on the two sides of the minimum, although the  $C$  vs  $E$  curves for all the NHEX concentrations explored merge with that of the supporting electrolyte at potentials negative of  $-1.3$  V and positive of  $-0.3$  V. Although thermodynamic analysis could be done from capacitance data extrapolating experimental results to 0 Hz, some qualitative findings are drawn from capacitance data observed from 5 to 150 Hz. If we integrate the  $C$  vs  $E$  curves (20 Hz) starting from any of these two extreme potentials, where NHEX desorption is complete, and we force the resulting curves of the charge density  $\sigma_M$  vs  $E$  to coincide at one of these two extremes, they will not coincide on the other extreme. This behavior denotes an irreversible adsorption and/or an adsorption-desorption step which is slow in the time scale of  $(20 \text{ Hz})^{-1}$ . In what follows, evidence will be provided by chronocoulometry that irreversible adsorption of NHEX molecules takes place only at the lowest NHEX concentrations, while a slow desorption of these molecules at positive potentials occurs at all NHEX concentrations explored.

As the NHEX concentration ( $c$ ) is progressively increased, the differential capacity minimum becomes lower and broader, while well-defined desorption peaks of increasing height develop on the two sides of the minimum. The differential capacity minimum in the presence of NHEX is slightly shifted on the negative side with respect to the pzc in the absence of NHEX. The frequency dispersion is small in the proximity of the differential capacity minimum, whereas it increases notably at the desorption peaks, as expected. Therefore, the capacity data cannot be used for a quantitative investigation of the adsorption of NHEX.

**Charge Measurements.** Capacitive charge measurements by the chronocoulometric technique were carried out by holding the applied potential at an initial value ( $E$ ) at which the solute is adsorbed for a time long enough to attain adsorption equilibrium; the applied potential was then stepped to a final value ( $E_f$ ) at which desorption takes place rapidly and completely, i.e. the current [ $i(t)$ ] following this potential step is zero after a few milliseconds. Electronic integration of this transient yields the corresponding charge [ $Q(t)$ ]. The experimental strategy in charge measurements is described thoroughly in refs 21

and 22 for measurements at a mercury drop and in ref 23 for measurements on solid electrodes.

The method can be successfully applied if no faradaic process takes place at the  $E_f$ , which is generally an extreme negative or positive potential chosen outside the potential range where the substance under study is adsorbed. Then the contribution to charge is purely capacitive.

It should be noted that no correction for a faradaic contribution can be regarded as entirely satisfactory if a disturbing electrode process yields a product which is adsorbed on the electrode surface, thus interfering with the adsorption of the substance under investigation. However, the faradaic complication can be overcome not only in the trivial case in which the disturbing faradaic process is slow in the time scale adopted but also in the more significant case in which the process is not diffusion controlled and hence gives rise to a constant current density. In this case the resulting  $Q(t)$  increases linearly in time and a linear extrapolation to  $t = 0$  corrects satisfactorily for the faradaic contribution, provided that the latter contribution is negligible during the very short time (1–2 ms) required for the imposed potential to switch from the initial to the final value.

For each NHEX concentration investigated two different chronocoulometric measurements were carried out in sequence: with both measurements the initial potential ( $E$ ) was varied between  $-1.3$  and  $-0.3$  V by 20 mV steps, but the final potential ( $E_f$ ) was set alternatively equal to  $-1.2$  and  $-0.1$  V. The time required for attaining adsorption equilibrium at  $E$  under mild stirring was found to be less than 10 s over the whole range of potentials and NHEX concentrations investigated. Hence each measurement was carried out by stirring the solution at each  $E$  value for 10 s, blocking the stirring 2 s before the potential step  $E \rightarrow E_f$ , holding the potential at  $E_f$  for 100 ms, and then stepping the potential back to the new initial value of  $E$ . This cycle was repeated under computer control until the whole range of  $E$  values was covered. The charge  $Q(E, t)$  was sampled at 1 ms intervals starting from the instant  $t = 0$  of each potential step ( $E \rightarrow E_f$ ). The time required for attaining adsorption equilibrium is much less than that reported by Vitanov and Popov<sup>12</sup> for the same system.

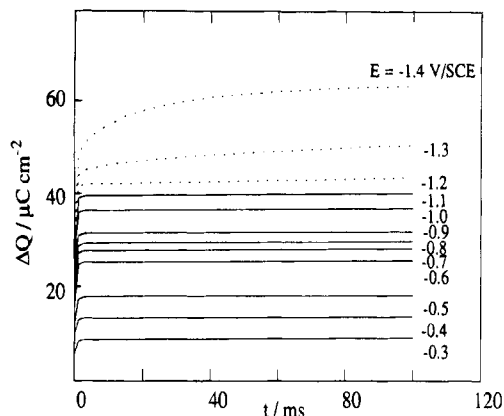
By proper adjustment of the positive feedback circuitry, the charge  $Q(E, t)$  following the potential step  $E \rightarrow E_f$  attained a practically time-independent value in a few milliseconds when  $E_f$  was set equal to  $-0.1$  V; this indicates that no detectable faradaic processes occur at this final potential in the 100 ms time window (see Figure 2). Conversely, the  $Q(E, t)$  vs  $t$  curves recorded by setting  $E_f = -1.2$  V exhibit a slight constant slope due to a mild hydrogen evolution which occurs at  $-1.2$  V. At any rate, the correction for this faradaic contribution by linear extrapolation of  $Q(E, t)$  to  $t = 0$  is quite accurate and is entirely justified in view of the lack of hydrogen adsorption on silver. The extrapolation to  $t = 0$  of the  $Q(E, t)$  values sampled over the time interval from  $t = 50$  to 100 ms after the potential step  $E \rightarrow E_f$  will be denoted by  $Q(E \rightarrow E_f)$ .

Figure 3 shows the  $Q(E \rightarrow E_f)$  vs  $E$  curves obtained in 0.05 M  $\text{KClO}_4$  by setting  $E_f$  equal to  $-0.1$  and  $-1.2$  V, respectively. Both curves were converted into  $\sigma_M$  vs  $E$  curves by setting  $Q(E \rightarrow E_f)$  equal to zero at the pzc as estimated from the minimum of the corresponding differential capacity curve. It is apparent that the two curves overlap exactly over a broad intermediate potential range, while they differ somewhat at the extreme potentials. In

(21) Foresti, M. L.; Moncelli, M. R.; Aloisi, G.; Carla', M. *J. Electroanal. Chem.* **1988**, *255*, 267.

(22) Foresti, M. L.; Pezzatini, G.; Monteagudo, J. C. G. *J. Electroanal. Chem.* **1990**, *295*, 251.

(23) Richer, J.; Lipkowski, J. *J. Electrochem. Soc.* **1986**, *133*, 121.



**Figure 2.** Plots of  $\Delta Q$  vs  $t$  for 0.02 M NHEX in 0.05 M  $\text{KClO}_4$ . The curves refer to different initial potentials,  $E_i$ , and one final potential,  $E_f = -0.1$  V. Dashed curves refer to potentials at which hydrogen evolution interferes and were therefore discarded in our analysis.

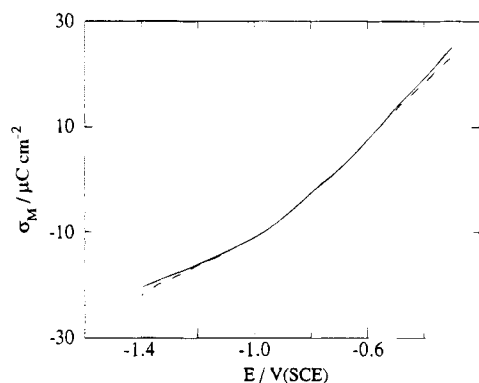


**Figure 3.** Plots of  $\sigma_M$  vs  $E$  for 0.05 M  $\text{KClO}_4$  in the absence of NHEX obtained as described in the text at an Ag(111) single crystal electrode which had been working for a long time by setting  $E_f$  equal to  $-0.1$  V (dashed curve) and to  $-1.2$  V (solid curve).

particular, the absolute values of  $\sigma_M$  are greater for  $E_f = -0.1$  V than for  $E_f = -1.2$  V at the more negative potentials, whereas they are smaller at the more positive potentials. This behavior can be explained by considering the way in which these  $\sigma_M$  values were obtained. When the electrode is held at the more negative  $E$  values for 10 s, a detectable amount of hydrogen is formed at its surface: if we step the potential to a final value  $E_f = -1.2$  V, this hydrogen will remain unaltered, but if we step the potential to  $E_f = -0.1$  V, it will be instantaneously reoxidized, thus increasing slightly the positive charge  $Q(E \rightarrow -0.1$  V) involved in this step with respect to its pure capacitive contribution. In addition, the high  $\text{OH}^-$  concentration created at the electrode surface entails an increase in the measured charge, due to  $\text{OH}^-$  adsorption.<sup>24</sup> In this respect the  $\sigma_M$  values at the more negative potentials are more reliable if they are obtained by setting  $E_f = -1.2$  V. On the other hand, when the electrode is kept at more positive  $E$  values for 10 s, a slight amount of silver oxide is formed on its surface: if we step the potential to  $E_f = -0.1$  V, this oxide will remain unaltered; in addition, more oxide will be formed during the holding time at  $-0.1$  V (100 ms). However, if we step the potential to  $E_f = -1.2$  V, this oxide will be instantaneously reduced, with a resulting slight increase in the negative charge  $Q(E \rightarrow -1.2$  V) involved in this step with respect to its pure capacitive contribution. In this respect the  $\sigma_M$  values at the more

positive potentials are determined conveniently by setting  $E_f = -0.1$  V.

When starting from a freshly prepared single crystal electrode or from an electrode entirely restored by mechanical polishing and annealing of the single crystal face, we have constantly observed that the discrepancies pointed out in Figure 3 increase with the repeated use of the electrode in adsorption measurements of the alcohol. Thus, a freshly prepared electrode or an electrode employed in only a few series of adsorption measurements would yield  $\sigma_M$  vs  $E$  curves of the supporting electrolyte as obtained by the two different procedures which practically coincided over the whole potential range from  $-1.3$  to  $-0.3$  V: the two curves in Figure 3 were indeed obtained at an electrode which had been used for several sets of measurements. The above experimental observations strongly suggest that the repeated use of a silver single crystal electrode in measurements of specific adsorption increases the density of surface defects which are not completely removed by the chemical polishing with  $\text{CrO}_3$  and which constitute preferential sites for hydrogen evolution and surface oxide formation. Therefore, the experimental data reported herein were obtained on electrodes which were either freshly prepared or had been employed in no more than three or four series of adsorption measurements.

An increase in the NHEX concentration causes a modest but appreciable increase in the rate of hydrogen evolution at  $E$  values negative of ca.  $-1.15$  V, as indicated by the increase in the slope of  $Q(t)$  vs  $t$  curves obtained by stepping to these potentials. A gradual increase in  $c$  also causes an incipient increase and then a decrease in the rate of oxide formation at  $E$  values positive of ca.  $-0.4$  V. Thus, the charge densities  $Q(E \rightarrow -1.2$  V) obtained at the latter  $E$  values first increase slightly over the corresponding charge values for the supporting electrolyte alone and then decrease: this behavior denotes an increase and then a decrease in the faradaic contribution to  $Q(E \rightarrow -1.2$  V) due to surface oxide formation. Since at potentials negative of  $-1.15$  V and positive of  $-0.4$  V the differential capacity curves of Figure 1 point to an almost complete desorption of NHEX, the above effects are probably to be ascribed to the catalytic action of alcohol molecules irreversibly adsorbed on the surface defects existing on the electrode surface. This hypothesis is supported by the observation that the lowest NHEX concentrations depress the differential capacity curves in the region of the minimum (see Figure 1), while they do not increase them on the two sides of the minimum: this suggests that the lowest NHEX concentrations tend to saturate the surface defects almost completely, while adsorption on the terraces is still quite low. Further evidence in favor of this interpretation is provided by the effect of the first NHEX additions, performed by regular logarithmic increments  $\Delta \log c \approx 0.1$ , on the curves of the absolute charge density ( $\sigma_M$ ) against  $E$  and on the corresponding curves of the interfacial tension ( $\gamma$ ) against  $E$ : the first addition of NHEX causes a change in  $\sigma_M$  (see Figure 4) and a depression in  $\gamma$  which are greater than those produced by the subsequent addition. This has led us to discard the  $\sigma_M$  vs  $E$  curve of the supporting electrolyte in the thermodynamic analysis of the experimental data.

We already stated that the charge densities  $Q(E \rightarrow -1.2$  V) are not complicated by hydrogen evolution at extreme negative potentials, whereas the charge densities  $Q(E \rightarrow -0.1$  V) are not complicated by surface oxide formation at extreme positive potentials. In view of these observations, the following strategy was adopted to obtain reliable  $\sigma_M$  vs  $E$  curves at the different NHEX concentrations. The two curves of  $Q(E \rightarrow -0.1$  V) vs  $E$

(24) Hamelin, A.; Morin, S.; Lipkowski, J. *J. Electroanal. Chem.* **1991**, *304*, 195.

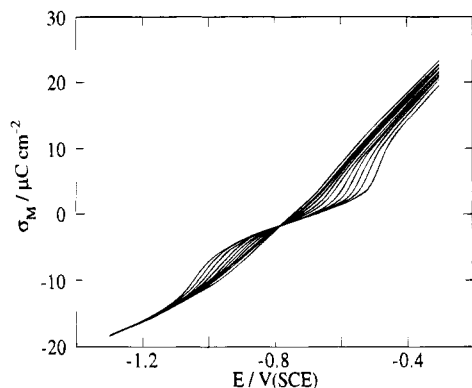


**Figure 4.** In passing from the steepest to the flattest curve over the intermediate potential region, the first curve is the  $\sigma_M$  vs  $E$  plot for the interface between Ag(111) and aqueous 0.05 M  $\text{KClO}_4$  in the absence of NHEX; the successive curves are relative to progressive additions of NHEX from  $4.35 \times 10^{-3}$  to  $3.46 \times 10^{-2}$  M by  $\log(c/M)$  increments of 0.1.

and of  $Q(E \rightarrow -1.2 \text{ V})$  vs  $E$  relative to the same  $c$  value were first shifted along the vertical axis with respect to each other so as to put them in coincidence over the broad intermediate potential range from ca.  $-1.0$  to ca.  $-0.6 \text{ V}$ . At potentials negative of this range, where the two curves diverge, only the  $Q(E \rightarrow -1.2 \text{ V})$  vs  $E$  curve was retained; conversely, at potentials positive of this range only the  $Q(E \rightarrow -0.3 \text{ V})$  vs  $E$  curve was retained. The  $Q(E)$  vs  $E$  curve for the supporting electrolyte so obtained was then converted into the corresponding curve of the absolute charge density  $\sigma_M$  vs  $E$  by setting  $Q(E)$  equal to zero at the pzc, as estimated from the minimum in the corresponding differential capacity curve. All other  $Q(E)$  vs  $E$  curves relative to the various NHEX concentrations were finally made to coincide with that of the supporting electrolyte at the more negative potentials, where NHEX is completely desorbed. Figure 4 shows a whole set of  $\sigma_M$  vs  $E$  curves obtained by this procedure. All these curves intersect at a single point, whose coordinates locate the charge,  $\sigma_M = -1.65 \mu\text{C cm}^{-2}$ , and the potential,  $E_m = -0.788 \text{ V}$ , of maximum adsorption. Unfortunately, even by following this procedure, the curves do not merge at  $-0.3 \text{ V}$ , but rather they run almost parallel over the extreme positive potential range explored. This agrees with the differential capacity curves of Figure 1 coinciding over the same potential range. This behavior is probably ascribable to a slow desorption in the time scale of 100 ms as we step to the positive final potential  $E_f = -0.1 \text{ V}$ . Incidentally, a slow desorption at potentials positive to the adsorption region has been reported for ethyl ether on Ag(111) and Ag(100) by Hinnen et al.<sup>11</sup> and for *tert*-pentyl alcohol on Au(111) by Richer et al.<sup>9</sup> Since the  $\sigma_M$  vs  $E$  curves obtained with  $E_f = -1.2 \text{ V}$ , at which potential desorption is fast, are almost exactly superimposable on the curves obtained with  $E_f = -0.1 \text{ V}$  over the potential range from ca.  $-1.0$  to ca.  $-0.6 \text{ V}$ , we are led to conclude that the rate of desorption following a potential step  $E \rightarrow -0.1 \text{ V}$  decreases progressively and rapidly with a decrease in the width of this step. For the above reasons, results obtained at potentials positive to  $-0.6 \text{ V}$  will not be taken into account in the further data treatment.

**Thermodynamic Analysis.** The thermodynamic analysis of the experimental curves of  $\sigma_M$  vs  $E$  was carried out by an entirely numerical procedure<sup>25</sup> using molar concentrations in place of activities; such a tactic is expected to produce a practically negligible error at the

relatively low NHEX concentrations investigated.<sup>26</sup> The surface excesses  $\Gamma(E, c)$ , were obtained by numerical differentiation with respect to  $\ln c$  of the interfacial tension values  $\gamma(E, c)$ . These curves were obtained by integration with respect to  $E$  of the directly measured  $\sigma_M(E, c)$  values. In calculating the isotherms at constant charge, Parsons' function  $\xi(E, c) = \gamma + \sigma_M E$  was first obtained. The surface excesses  $\xi(\sigma_M, c)$  were then calculated by numerical differentiation of  $\xi(\sigma_M, c)$  with respect to  $\ln c$ .

The parameters for NHEX adsorption on Ag(111) from aqueous 0.05 M  $\text{KClO}_4$  are summarized in Table 1, where they are compared with the parameters for NHEX adsorption on Hg from aqueous 0.1 M NaF.<sup>27</sup> The charge,  $\sigma_m$ , and the potential,  $E_m$ , of maximum adsorption were determined from the coordinates of the common intersection point of the  $\sigma_M$  vs  $E$  plots. The maximum surface concentration,  $\Gamma_m$ , was determined from the adsorption isotherm at  $E_m$ , which shows a distinct limiting value (see Figure 5). The differential capacity  $C_1$  at maximum coverage was obtained from the intercept of plots of the differential capacity  $C$  at  $E = E_m$  against  $\Gamma$  on the  $\Gamma = \Gamma_m$  axis, as described in ref 28. The potential of zero charge at maximum coverage was obtained by determining the intercepts on the  $\sigma_M = 0$  axis of the linear sections of the  $\sigma_M$  vs  $E$  plots about  $E = E_m$  at alcohol concentrations corresponding to  $\theta = \Gamma/\Gamma_m$  values greater than 0.5, by plotting these intercepts against  $\theta$  and by measuring the intercept of the resulting plot on the  $\theta = 1$  axis. The shift  $E_N$  of the potential of zero charge when passing from  $\theta = 0$  to 1 was then obtained by subtracting the potential charge at maximum coverage so obtained from the potential of zero charge,  $-0.746 \text{ V/SCE}$ , in the absence of the surfactant.

The standard Gibbs energy of adsorption at zero coverage,  $\Delta G^\circ_{\text{ads}}$ , as a function of the applied potential  $E$  was obtained by fitting the experimental isotherms at constant potential to the Frumkin isotherm:

$$\frac{c}{55.5} \exp\left(-\frac{\Delta G^\circ_{\text{ads}}}{RT}\right) = \frac{\theta}{1-\theta} \exp(a\theta) \quad (1)$$

where  $a$  is the Frumkin interaction factor. Values of  $\Delta G^\circ_{\text{ads}}$  and  $a$  were thus obtained from the intercepts and slopes of the least-squares fittings to a straight line of  $\ln[c(1-\theta)/\theta]$  vs  $\theta$  plots at constant  $E$ , over the  $\theta$  range from 0.2 to 0.7. Figure 6 shows a plot of  $\Delta G^\circ_{\text{ads}}$  vs  $E$ , whereas the  $\Delta G^\circ_{\text{ads}}$  and  $a$  values at  $E = E_m$  are reported in Table 1. This table also reports values of the coefficients  $b_E = \partial(\Delta G^\circ_{\text{ads}}/RT)/\partial(E - E_m)^2$  for the quadratic dependence of the standard Gibbs energy of adsorption upon  $(E - E_m)$ , the superscripts + and - denoting whether the least-squares fitting to a straight line was made at negative or positive values of  $(E - E_m)$ . This fitting was confined to the lower  $(E - E_m)^2$  values, whenever appreciable deviations from linear behavior were observed at higher values.

The adsorption isotherm at constant charge obtained at  $\sigma_M = \sigma_m$  is practically identical to the corresponding isotherm at constant potential obtained at  $E = E_m$ . This is the obvious consequence of the independence of the intersection point of the  $\sigma_M$  vs  $E$  curves upon the alcohol concentration, which causes the potential  $E$  to remain practically constant at  $E_m$  when  $\sigma_M$  is kept constant at  $\sigma_m$ .

(26) Moncelli, M. R.; Foresti, M. L.; Guidelli, R. *J. Electroanal. Chem.* **1990**, *295*, 225.

(27) Foresti, M. L.; Moncelli, M. R. *J. Electroanal. Chem.* **1993**, *348*, 429.

(28) Moncelli, M. R.; Foresti, M. L. *J. Electroanal. Chem.* **1993**, *359*, 293.

(25) Carla', M.; Aloisi, G.; Foresti, M. L.; Guidelli, R. *J. Electroanal. Chem.* **1986**, *197*, 123.

**Table 1.** Parameters for NHEX Adsorption on Ag(111) from Aqueous 0.05 M KClO<sub>4</sub> and on Hg from Aqueous 0.1 M NaF

parameter	Ag(111) (this work)	Hg <sup>27</sup>	parameter	Ag(111) (this work)	Hg <sup>27</sup>
$10^{-10}\Gamma_m/\text{mol cm}^{-2}$	2	3.4	$(\Delta G^\circ_{\text{ads}})_{\text{min}}/\text{kJ mol}^{-1}$	-18.4 <sup>a</sup>	-23.8 <sup>a</sup>
$A/\text{nm}^2$		0.49	$a (E = E_m)$	$\sim -2.9$	-2.6
$\sigma_m/\mu\text{C cm}^{-2}$	-1.65	-1.9	$b_E^+/\text{V}^{-2}$	35	10.8
$E_m/\text{V (SCE)}$	-0.788	-0.520	$b_E^-/\text{V}^{-2}$	28	8.1
$C_1/\mu\text{F cm}^{-2}$	14	6.2	$b_\sigma^+/\text{cm}^4 \mu\text{C}^{-2}$	0.037	0.029
$E_N/\text{V}$	0.060	0.185	$b_\sigma^-/\text{cm}^4 \mu\text{C}^{-2}$	0.023	0.021

<sup>a</sup> The standard state for the solvent is the pure solvent, and that for the solute is the hypothetical ideal pure substance in both bulk and adsorbed states.

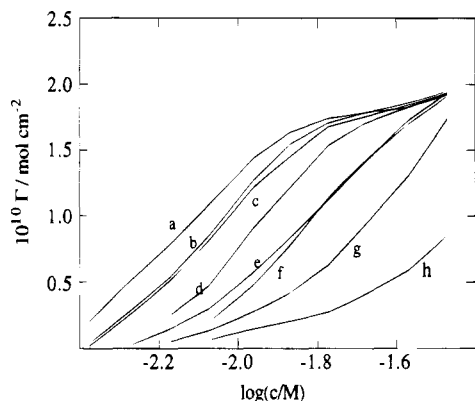


**Figure 5.** Plots of  $\Gamma$  vs  $\log c$  at constant  $E$  relative to NHEX adsorption on Ag(111) from aqueous 0.05 M KClO<sub>4</sub> for  $E$  values equal to -0.780 (a), -0.860 (b), -0.700 (c), -0.660 (d), -0.940 (e), -0.620 (f), -0.980 (g), and -1.020 V (h).

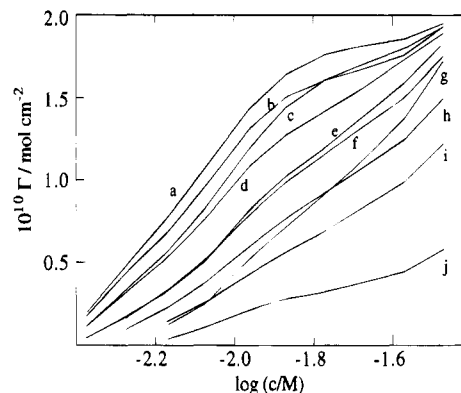


**Figure 7.** Plots of  $\Gamma$  vs  $\log c$  at constant  $\sigma_M$  relative to NHEX adsorption on Ag(111) from aqueous 0.05 M KClO<sub>4</sub> for  $\sigma_M$  values equal to -2 (a), 0 (b), -4 (c), 1 (d), 2 (e), -6 (f), 3 (g), -7 (h), -8 (i), and -10  $\mu\text{C cm}^{-2}$  (j).

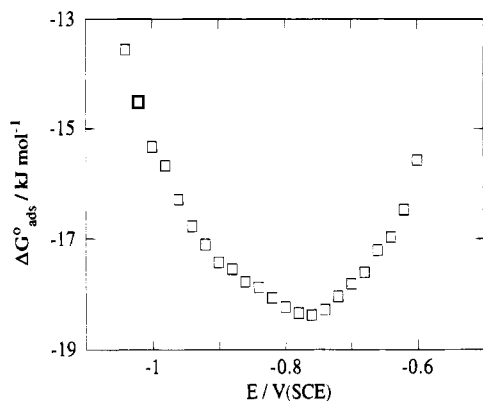


**Figure 6.** Plot of  $\Delta G^\circ_{\text{ads}}$  vs  $E$  for NHEX adsorption on Ag(111) from aqueous 0.05 M KClO<sub>4</sub>.

The  $\Delta G^\circ_{\text{ads}}$  and  $a$  values at the constant charge  $\sigma_M = \sigma_m$  as obtained from the intercept and slope of the  $\ln[c(1 - \theta)/\theta]$  vs  $\theta$  plot at  $\sigma_m$  are therefore practically identical to the corresponding values at the constant potential  $E = E_m$ . However, as we depart from the charge of maximum adsorption,  $\sigma_m$ , the  $\Gamma$  vs  $\log c$  plots at constant charge density tend to an apparent limiting value which decreases progressively with increasing  $|\sigma_M - \sigma_m|$ , as shown in Figure 7. This behavior of the adsorption isotherms at constant charge as compared to that of the isotherms at constant potential is observed for practically all simple aliphatic compounds (see, for instance, the  $\Gamma$  vs  $\log c$  curves at constant  $E$  and  $\sigma_M$  for *n*-pentanol adsorption from aqueous 0.5 M Na<sub>2</sub>SO<sub>4</sub> in Figures 3 and 4 of ref 26). As a consequence of this behavior, the  $\ln[c(1 - \theta)/\theta]$  vs  $\theta$  plots at constant charge as obtained by setting  $\theta = \Gamma/\Gamma_m$ , with  $\Gamma_m$  derived from the adsorption isotherm at  $\sigma_M = \sigma_m$ , show increasing deviations from linear behavior and a progressive decrease in the average value of their slope with an increase in  $|\sigma_M - \sigma_m|$ . Due to these large deviations, no attempt was made to estimate Frumkin interaction factors  $a$  at constant charge for charges  $\sigma_M \neq \sigma_m$ . Moreover,  $\Delta G^\circ_{\text{ads}}$  values at constant  $\sigma_M$  were obtained by linear extrapolation

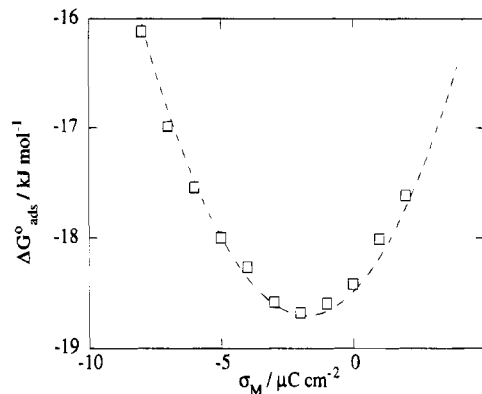


**Figure 8.** Plot of  $\Delta G^\circ_{\text{ads}}$  vs  $\sigma_M$  for NHEX adsorption on Ag(111) from aqueous 0.05 M KClO<sub>4</sub>. The dashed curve was calculated as described in the text.

to  $\theta = 0$  of the lower portion of  $\ln[c(1 - \theta)/\theta]$  vs  $\theta$  plots at constant charge, i.e. the portion from  $\theta = 0.1$  to 0.4. Figure 8 shows a plot of  $\Delta G^\circ_{\text{ads}}$  vs  $\sigma_M$ . Table 1 reports values of the coefficients  $b_\sigma = \partial(\Delta G^\circ_{\text{ads}}/RT)/\partial(\sigma_M - \sigma_m)^2$  for the quadratic dependence of the standard Gibbs energy of adsorption upon  $(\sigma_M - \sigma_m)$ , where the superscripts + and - denote whether the least-squares fitting to a straight line was made at negative or positive values of  $(\sigma_M - \sigma_m)$ . The ratios  $(b_\sigma^+/b_\sigma^-)^{1/2}$  are in the range from 31 to 35  $\mu\text{F cm}^{-2}$  and are therefore relatively close to the differential capacity  $C_0$  of the Ag(111)/electrolyte interface in the absence of surfactants, in accordance with predictions.<sup>26</sup>

## Discussion

The  $\Gamma_m$  value for NHEX on Ag(111) is appreciably less than the value,  $\approx 3.95 \times 10^{-10}$  mol cm<sup>-2</sup>, corresponding to full coverage of NHEX, calculated for molecules in a flat orientation, area = 0.42 nm<sup>2</sup>, on the basis of a space-filling model.<sup>26</sup> In contrast, the experimental  $\Gamma_m$  value for NHEX adsorption on mercury as reported in Table 1 is close to this calculated value. The larger amount of

**Table 2. Standard Gibbs Energy of Adsorption (kJ mol<sup>-1</sup>) of NHEX at Metal/Water Interfaces at the Potential of Maximum Adsorption**

Hg	Bi	Sn	In(Ga)	Cd	Ag(111)	Zn	Ga
-23.8	-21.2	-21.1	-20.2	-19.4	-18.4	-18.3	-17.6

water molecules which remain adsorbed on silver when  $\Gamma$  reaches its limiting value points to a higher hydrophilicity of this metal with respect to mercury. Further evidence in favor of this conclusion is provided by the much more negative standard Gibbs energy of adsorption of NHEX on Hg,  $-23.8$  kJ mol<sup>-1</sup>.<sup>27</sup> As a matter of fact, the standard Gibbs energy of adsorption,  $\Delta G^\circ_{\text{ads}}$ , of a neutral compound which interacts weakly with metals can be used as a measure of their hydrophilicity, since the main difference in  $\Delta G^\circ_{\text{ads}}$  when passing from one metal to another can then be ascribed to the difference in the energy required to desorb the water molecules which must make room for the adsorbing compound. Table 2 summarizes  $\Delta G^\circ_{\text{ads}}$  values for NHEX adsorption from aqueous solutions on various sp metals as well as on Ag(111). Taking into account that an increment in the hydrocarbon chain length of *n*-aliphatic alcohols by one  $-\text{CH}_2-$  group is accompanied by a roughly constant increment in the negative value of  $\Delta G^\circ_{\text{ads}}$ , the  $\Delta G^\circ_{\text{ads}}$  values for NHEX on sp metals in Table 2 were obtained by linear extrapolation of the corresponding values for *n*-propanol, *n*-butanol, and *n*-pentanol available in the literature (see ref 29 for Ga, ref 27 for Hg, and ref 30 for all other sp metals). It can be seen that, according to this hydrophilicity scale, Ag(111) is nearly as hydrophilic as gallium, and hence turns out to be one of the most hydrophilic metals. A more detailed discussion is given in ref 31 for the (100) and (110) silver faces.

The difference in behavior of the adsorption isotherms at constant charge in Figure 7 with respect to those at constant potential in Figure 5 agrees with the predictions of a three-dimensional lattice model of TIP4P water molecules and of polar dimeric solute molecules against a charged wall, recently developed in our laboratory.<sup>32</sup> The model, which does not make use of molecules, represents solute molecules as dimers consisting of a nonpolar segment, which simulates a very short hydrocarbon chain, and of a polar segment, which simulates the polar head. This model predicts that the surface concentration,  $\Gamma$ , at constant charge increases with  $\log c$ , tending to an ill-defined apparent limiting value less than  $\Gamma_m$ , which is lower the more the charge departs from its value of maximum adsorption,  $\sigma_m$ . This behavior<sup>32</sup> is explained by the fact that the local electric field anchoring the water molecules to the electrode surface consists of the external field  $4\pi\sigma$  plus the additional polarization field created by the neighboring water molecules, which acts in the direction opposite to the external electric field. As the surface coverage  $\theta$  increases, the polarization field decreases accordingly, and hence the local field at constant charge increases in absolute value, approaching  $4\pi\sigma$ . Hence, the residual adsorbed water molecules will be held in the adsorbed state by the local field more tightly the higher is  $\theta$ ; this explains the attainment of an apparent limiting value of the surface coverage, albeit ill-defined, which decreases with increasing  $|\sigma|$ . No such a behavior is predicted when it is the applied potential  $E$  which is

held constant. In fact, the imposed constancy of  $E$  requires a gradual decrease in the absolute value of the external electric field  $4\pi\sigma$  with increasing  $\theta$ , in order to compensate for the gradual decrease in the absolute value of the counterfield produced by the adsorbed water molecules. Therefore, at constant  $E$  the progressive increase in  $\theta$  does not cause the residual adsorbed water molecules to be more strongly anchored to the surface as in the case of constant  $\sigma_m$ , and hence  $\Gamma_m$  turns out to be practically independent of  $E$ . The penalty which one has to pay in using the above refined three-dimensional lattice model, which does not make use of adjustable parameters,<sup>32</sup> is the difficulty of predicting the adsorption behavior of *n*-aliphatic compounds having a long hydrocarbon chain, due to the notable increase in the complexity of the statistical mechanical treatment of the model with an increase in the number of monomeric segments composing the solute molecule.

For a quantitative comparison between experimental behavior and modelistic predictions, we shall adopt another model of adsorbed water monolayer and solute molecules in which the water molecules interact with each other via H-bonds and dipole-dipole forces, whereas solute molecules interact with each other and with water molecules via dipole-dipole forces only.<sup>33</sup> This model makes use of two adjustable parameters to fit experimental results, namely the number ( $n$ ) of adsorbed water molecules displaced by one adsorbing solute molecule and the normal component ( $\mu_N$ ) of the dipole moment of the adsorbed solute molecules. The unknown values of  $n$  and  $\mu_N$  are obtained from the experimental values of  $\sigma_m$  and  $b_\sigma^-$  by making use of a calculated plot of the  $\mu_N/n$  ratio vs  $\sigma_m$  to obtain  $\mu_N/n$  and then of calculated plots of  $\mu_N/n$  vs  $b_\sigma^-$  at different  $n$  values to obtain  $n$ .<sup>26,34</sup> In the present case (NHEX) the estimated value of the  $\mu_N/n$  ratio is close to  $-0.3$  D. Confining ourselves to  $n$  values which are multiples of 0.5, the resulting  $n$  value equals 4, and hence coincides with the value estimated for NHEX adsorption on Hg<sup>26</sup> on the basis of the same model. This  $n$  value complies satisfactorily with the surface area,  $0.42$  nm<sup>2</sup>, estimated for a NHEX molecule in a flat orientation when we consider that the area projected by one adsorbed water molecule is close to  $0.10$  nm<sup>2</sup>. This result supports the point of view that the NHEX molecules are adsorbed in a flat orientation on Ag(111) as well as on Hg, at least at low surface coverages; moreover, their dipole moment normal component ( $\mu_N$ ) is approximately the same on both electrode materials. The negative value of  $\mu_N$  implies that the NHEX molecule is adsorbed with the positive end of its dipole toward the metal; this justifies the positive value of  $60$  mV for the shift  $E_N$  of the pzc when passing from  $\theta = 0$  to 1, also in view of the fact that the water dipoles are expected to turn their negative end toward the metal in the proximity of the pzc.

The model adopted herein for the estimate of the  $\mu_N$  and  $n$  values<sup>33</sup> predicts an adsorption behavior at constant charge which is in fairly good agreement with the Frumkin isotherm of eq 1, at least for  $\theta \leq 0.7$ . Hence, fitting  $\ln[c(1 - \theta)/\theta]$  vs  $\theta$  plots calculated from the model to a straight line over the  $\theta$  range from 0 to 0.7 yields an intercept on the  $\theta = 0$  axis which measures the standard Gibbs energy of adsorption at zero coverage,  $\Delta G^\circ_{\text{ads}}$ , apart from an additive constant; moreover, the slope of this straight line provides a value for the interaction factor  $\alpha$  to be compared with the experimental one. The dashed curve in Figure 8 is a plot of  $\Delta G^\circ_{\text{ads}}$  against  $\sigma$  calculated from the model for  $\mu_N/n = -0.3$  D and  $n = 4$ ; this curve was shifted along

(29) Pezzatini, G.; Moncelli, M. R.; Innocenti, M.; Guidelli, R. *J. Electroanal. Chem.* **1990**, *295*, 275.

(30) Trasatti, S. In *Modern Aspects of Electrochemistry*; Conway, B. E.; Bockris, J. O'M., Eds.; Plenum Press: New York, 1979; Vol 13, p 81.

(31) Foresti, M. L.; Innocenti, M.; Guidelli, R. *J. Electroanal. Chem.* **1994**, *376*, 85.

(32) Guidelli, R.; Aloisi, G. *J. Electroanal. Chem.* **1992**, *329*, 39.

(33) Guidelli, R.; Foresti, M. L. *J. Electroanal. Chem.* **1986**, *197*, 103.

(34) Moncelli, M. R.; Pezzatini, G.; Guidelli, R. *J. Electroanal. Chem.* **1989**, *272*, 217.

the vertical axis so as to obtain the best overlap with the corresponding experimental curve. The  $a$  value calculated from the model,  $-3.7$ , is somewhat greater than the corresponding experimental value.

The differential capacity  $C_1$  at maximum coverage on the Ag(111) face,  $14 \mu\text{F cm}^{-2}$ , is relatively high when compared with the corresponding value on mercury,  $6.2 \mu\text{F cm}^{-2}$ .<sup>27</sup> This higher  $C_1$  may be due partly to the presence of surface defects which increase the real area of the electrode surface with respect to the geometric area. However, the ratio of these two areas is expected to be hardly greater than 1.1.<sup>35</sup> A further cause of the increase of  $C_1$  in passing from Hg to Ag is due to the fact that the water content in the adsorbed film at maximum coverage is greater on Ag than on Hg. Thus, the presence of water in the adsorbed monomolecular film may increase the distortional dielectric constant ( $\epsilon$ ) of the film<sup>36,37</sup> and/or decrease its average thickness ( $\delta$ ):<sup>22,38</sup> both effects tend to increase  $C_1$  in view of the well-known expression  $C = \epsilon/(4\pi\delta)$  for the capacity of a parallel-plate capacitor. Another factor for  $C_1$  being greater on Ag than on Hg may be ascribed to the fact that the negative contribution,  $C_{\text{el}}^{-1}$ , from electron spillover to the reciprocal ( $C_0^{-1}$ ) of the differential capacity at zero coverage is probably greater for Ag than for Hg. Roughly speaking, this negative contribution is greater the larger the polarizability of the "electronic tail", which in turn is expected to increase with an increase in the bulk density of free electrons. The problem of the effective density of free electrons is complicated in the case of sd metals, because the d electrons in these metals can neither be considered as free nor as bound. Schmickler and Henderson<sup>39</sup> estimated

the electron density of Ag to be much closer to the high value for Ga than to the relatively low value for Hg. However, it must be considered that the relative weight of the  $C_{\text{el}}^{-1}$  contribution to  $C_1^{-1}$  is certainly less than that to  $C_0^{-1}$ , since  $C_1^{-1} > C_0^{-1}$ .

So far discussion was based on the model described by Guidelli and co-workers.<sup>32,33</sup>

Recent experimental findings about ordering of water at the Ag(111)/NaF interface<sup>40</sup> by in-situ SXRS (surface X-rays scattering) suggest not only reorientation of water dipoles when the sign of the charge on the metal changes but also a change of a real density in the first layer from 1.1 at  $-10 \mu\text{C cm}^{-2}$  to 1.8 at  $25 \mu\text{C cm}^{-2}$ . Our base electrolyte was  $\text{KClO}_4$ , not NaF, therefore these findings cannot be directly introduced in our results; furthermore, it is difficult to foresee what would be the influence of NHEX adsorption on these large first-layer water densities. These SXRS observations demonstrate that there is no change in the atomic surface structure of Ag(111) from  $-10$  to  $25 \mu\text{C cm}^{-2}$ , i.e. no reconstruction, but only a small contraction between the top and second layer of silver atoms at the more positive charges. Therefore, the potential steps are performed all along our experiment on the same superficial atomic structure, it is not the case for faces which reconstruct, low-index gold faces for instance.

**Acknowledgment.** The authors wish to thank Mr. Ferdinando Capolupo and Mr. Andrea Pozzi for valuable technical assistance. The financial support of the MURST and of the Italian CNR is gratefully acknowledged.

LA9403789

(35) Foresti, M. L.; Guidelli, R.; Hamelin, A. *J. Electroanal. Chem.* **1993**, *346*, 73.

(36) Damaskin, B. B.; Survila, A. A.; Rybalka, L. E. *Elektrokhimiya*, **1967**, *3*, 146.

(37) Schumann, D. *J. Electroanal. Chem.* **1986**, *201*, 247.

(38) Carla', M.; Aloisi, G.; Moncelli, M. R.; Foresti, M. L. *J. Colloid Interface Sci.* **1989**, *132*, 72.

(39) Schmickler, W.; Henderson, D. *J. Chem. Phys.* **1986**, *85*, 1650.

(40) Toney, M. F.; Howard, J. N.; Richer, J.; Borges, G. L.; Gordon, J. G.; Melroy, O. R.; Wiesler, D. G.; Yee, D.; Sorensen, L. B. *Nature* **1994**, *368*, 444.